Amorphous (Mo, Ta, or W)–Si–N diffusion barriers for Al metallizations

J. S. Reid,[a] E. Kolawa,[b] C. M. Garland, and M.-A. Nicolet
California Institute of Technology, Pasadena, California 91125

F. Cardone and D. Gupta
IBM Research Laboratories, Yorktown Heights, New York 10598

R. P. Ruiz
Jet Propulsion Laboratory, Pasadena, California 91109

(Received 16 January 1995; accepted for publication 29 September 1995)

M–Si–N and M–Si (M=Mo, Ta, or W) thin films, reactively sputtered from M_5Si_3 and WSi_2 targets, are examined as diffusion barriers for aluminum metallizations of silicon. Methods of analysis include electrical tests of shallow-junction diodes, $^4He^{++}$ backscattering spectrometry, x-ray diffraction, transmission electron microscopy, scanning electron microscopy, and secondary-ion-mass spectrometry. At the proper compositions, the M–Si–N films prevent Al overlayers from electrically degrading shallow-junction diodes after 10 min anneals above the melting point of aluminum. Secondary-ion-mass spectrometry indicates virtually no diffusivity of Al into the M–Si–N films during a 700 °C/10 h treatment. The stability can be partially attributed to a self-sealing 3-nm-thick AlN layer that grows at the M–Si–N/Al interface, as seen by transmission electron microscopy. © *1996 American Institute of Physics.* [S0021-8979(96)01902-4]

I. INTRODUCTION

Preventing the interaction of aluminum interconnects and contacts with silicon, diffusion barriers are fundamental elements in many integrated circuits. Although widely investigated, only a marginal degree of stability has been achieved with most metal-nitride,[1–9] boride,[10–13] oxide,[6,14,15] and carbide[16–20] barriers because aluminum reacts with the vast majority of these interstitial compounds. Also reactive with Al, many amorphous barriers[21–26] have had no advantage over their polycrystalline counterparts, despite their supposed lack of fast diffusion paths. In contrast, exceptional performance has been achieved with amorphous Ta–Si–N ternary alloys, which prevent Al from breaching the barrier at temperatures above the melting point of Al, 660 °C.[27,28] In those studies, Ta–Si–N reportedly did not react with Al, according to x-ray diffraction and conventional transmission electron microscopy (TEM) analyses. Curiously, tantalum silicides,[27] tantalum nitrides,[8] and silicon nitride[29–31] are all known to react with Al. In this article we show that W–Si–N and Mo–Si–N are also effective barriers. Through high-resolution transmission electron microscopy of W–Si–N/Al bilayers and secondary-ion-mass spectrometry of Ta–Si–N/Al/Ta–Si–N trilayers, we offer an explanation for the high stability. For comparative purposes, nitrogen-free amorphous Mo-, Ta-, and W-silicide barriers are also evaluated.

II. PROCEDURE

Four different substrates were used for our experiments: unpatterned (100) silicon and oxidized silicon for ^{4}He backscattering, x-ray, scanning electron microscopy (SEM), and secondary-ion-mass spectrometry (SIMS) analyses; graphite for compositional determination by backscattering, photoresist-patterned silicon containing vertical n^+p shallow-junction diodes; and single-crystal NaCl substrates for transmission electron microscopy. The lateral contact area and junction depth of the diodes are $250\times250\ \mu m^2$ and 280 nm, respectively. The junctions were formed by implanting 8×10^{15} As^+ into a 30–50 Ω cm, p epilayer on a p^+ substrate. All depositions were performed by 13.56 MHz sputtering in a chamber evacuated to $1–4\times10^{-7}$ Torr vacuum by means of a cryopump and cryogenic baffle. Throttling the pump for deposition raised the base pressure to almost 10^{-6} Torr. The sputtering source was a 7.5-cm-diam, 300 W rms cathode with a fixed magnetron. Just prior to loading into the chamber, the silicon samples were etched in 1:15 HF:H_2O. Thin films of M–Si and M–Si–N (M=Mo, Ta, or W) were deposited in Ar or Ar/N_2 discharges at 10 mTorr pressure from M_5Si_3 and WSi_2 targets. For most of the barrier depositions, the stage floated electrically. For the Mo–Si and Mo–Si–N depositions, a −115 V dc bias was applied to the stage to reduce oxygen content in the films. Without breaking vacuum, some samples additionally received an aluminum overlayer sputtered in an Ar discharge at 5 mTorr with a −50 V dc substrate bias. In most cases, the thickness of the barriers and aluminum was approximately 130 and 330 nm, respectively, as measured by stylus profilometry. The barrier thickness of 130 nm was chosen to facilitate many of the laboratory analyses but, as explained later in this article, much thinner barriers should perform equally well. Samples for TEM had both barrier and aluminum thicknesses of 50 nm. Samples for SIMS consisted of a Ta–Si–N (100 nm)/Al (6 nm)/Ta–Si–N (50 nm) trilayer on oxidized silicon. After deposition (and lift-off in acetone, where applicable), the samples were annealed for 10 min to 10 h in $<10^{-6}$ Torr vacuum and characterized by 2.0 MeV ^{4}He backscattering, Read-camera x-ray diffraction, and current versus voltage $I(V)$ measurements. Cross-sectional samples for TEM were lifted off of the NaCl in de-ionized H_2O,

[a]Present address: Intel Corporation, D1-67, Hillsboro, OR 97124-6497; Electronic mail: jreid@iago.caltech.edu
[b]Present address: Jet Propulsion Laboratory, 183-401, Pasadena, CA 91109.

Downloaded¬01¬Jun¬2006¬to¬131.215.240.9.¬Redistribution¬subject¬to¬AIP¬license¬or¬copyright,¬see¬http://jap.aip.org/jap/copyright.jsp

TABLE I. Deposition conditions, composition, resistivity, and highest stability temperature for diode tests.

Composition	$N_2/(Ar+N_2)$ flow ratio (%)	Resistivity ($\mu\Omega$ cm)	Max. stability temp.
Mo_5Si_3 target:			
$Mo_{74}Si_{26}$	0.0	180	400 °C/30 min
$Mo_{36}Si_{17}N_{47}$	28.5	1400	675 °C/10 min
W_5Si_3 target:			
$W_{80}Si_{20}$	0.0	200	400 °C/30 min
$W_{41}Si_{17}N_{42}$	15.0	790	550 °C/30 min
$W_{36}Si_{14}N_{50}$	25.0	1040	675 °C/10 min
WSi_2 target:			
$W_{44}Si_{56}$	0.0	300	400 °C/30 min
$W_{24}Si_{36}N_{40}$	16.7	1800	500 °C/30 min
Ta_5Si_3 target:			
$Ta_{80}Si_{20}$	0.0	260	400 °C/30 min
$Ta_{36}Si_{14}N_{50}$	7.8	625	675 °C/15 min

collected on a 200 mesh Mo grid coated with Si_3N_4, annealed in vacuum, recollected, and embedded in epoxy resin. After curing, the films in the epoxy were microtoned into roughly 50 nm sections through standard diamond-knife, ultramicrotomy techniques and collected on holey carbon films strung across a 200 mesh Cu grid.

III. RESULTS

A. M–Si barriers

The compositions and resistivities of the evaluated binary barriers are listed in Table I. All of the silicides have roughly 2 at. % each of argon and oxygen. The resistivities range from a low of 180 $\mu\Omega$ cm for $Mo_{74}Si_{26}$ to a high of 300 $\mu\Omega$ cm for the silicon-rich $W_{44}Si_{56}$. A summary of phases detected by x-ray diffraction after annealing of M–Si/Al bilayers on silicon or oxidized silicon substrates is given in Table II. The choice of substrate (Si or oxidized Si)

TABLE II. X-ray-diffraction summary of annealed barrier (130 nm)/Al (350 nm) bilayers on ⟨Si⟩ and SiO_2 substrates.

System	Process	Detected phases
Mo_5Si_3 target:		
⟨Si⟩ or $SiO_2/Mo_{74}Si_{26}/Al$	350 °C/30 min	amorphous Mo–Si, Al
	400 °C/30 min	$MoAl_{12}$, amorphous Mo–Si, Al
	450 °C/30 min	$MoAl_{12}$, amorphous Mo–Si, Al
	500 °C/30 min	$MoAl_{12}$, amorphous Mo–Si, Al
	550 °C/30 min	$MoAl_{12}$, Mo_4Al_{17}
⟨Si⟩ or $SiO_2/Mo_{36}Si_{17}N_{47}/Al$	600 °C/2 h	amorphous Mo–Si–N, Al
	625 °C/2 h	amorphous Mo–Si–N, Al, poly Si
$SiO_2/Mo_{36}Si_{17}N_{47}/Al$	700 °C/2 h	amorphous Mo–Si–N, Al, poly Si
W_5Si_3 target:		
⟨Si⟩ or $SiO_2/W_{80}Si_{20}/Al$	350 °C/30 min	amorphous W–Si, Al
	400 °C/30 min	WAl_{12}, amorphous W–Si, Al
	450 °C/30 min	WAl_{12}, amorphous W–Si, Al
	500 °C/30 min	WAl_{12}, $W(Si,Al)_2$, amorphous W–Si, Al
	550 °C/30 min	WAl_{12}, $W(Si,Al)_2$, Al
⟨Si⟩ or $SiO_2/W_{41}Si_{17}N_{42}/Al$	500 °C/30 min	amorphous W–Si–N, Al
	550 °C/30 min	WAl_{12}, amorphous W–Si–N, Al
	600 °C/30 min	WAl_{12}, amorphous W–Si–N, Al
⟨Si⟩ or $SiO_2/W_{36}Si_{14}N_{50}/Al$	600 °C/2 h	amorphous W–Si–N, Al
	625 °C/2 h	amorphous W–Si–N, Al, poly Si
$SiO_2/W_{36}Si_{14}N_{50}/Al$	700 °C/2 h	amorphous W–Si–N, Al, poly Si
WSi_2 target:		
⟨Si⟩ or $SiO_2/W_{44}Si_{56}/Al$	300 °C/30 min	amorphous W–Si, Al
	350 °C/30 min	WAl_{12}, amorphous W–Si, Al
	400 °C/30 min	WAl_{12}, amorphous W–Si, Al
	450 °C/30 min	WAl_{12}, amorphous W–Si, Al
	500 °C/30 min	WAl_{12}, $W(Si,Al)_2$, amorphous W–Si, Al
	550 °C/30 min	WAl_{12}, $W(Si,Al)_2$, Al
⟨Si⟩ or $SiO_2/W_{24}Si_{36}N_{40}/Al$	450 °C/30 min	amorphous W–Si–N, Al
	500 °C/30 min	WAl_{12}, amorphous W–Si–N, Al
	550 °C/30 min	WAl_{12}, amorphous W–Si–N, Al
Ta_5Si_3 target:		
⟨Si⟩ or $SiO_2/Ta_{80}Si_{20}/Al$	350 °C/30 min	amorphous Ta–Si, Al
	400 °C/30 min	Ta_3Al, amorphous Ta–Si, Al
	450 °C/30 min	Ta_3Al, amorphous Ta–Si, Al
	500 °C/30 min	Ta_3Al, amorphous Ta–Si, Al
	550 °C/30 min	Ta_3Al, amorphous Ta–Si, Al

Downloaded¬01¬Jun¬2006¬to¬131.215.240.9.¬Redistribution¬subject¬to¬AIP¬license¬or¬copyright,¬see¬http://jap.aip.org/jap/copyright.jsp

did not appear to alter the reaction products, as shown in Table II. Reacting at the lowest temperature, incipient reaction between $W_{44}Si_{56}$ and Al occurs during annealing at 350 °C/30 min to form WAl_{12}. At 400 °C, $W_{80}Si_{20}$, $Mo_{74}Si_{26}$, and $Ta_{80}Si_{20}$ react to produce WAl_{12}, $MoAl_{12}$, and $TaAl_3$. In these low-temperature cases, the reaction products provide very weak x-ray intensities, suggesting that only a small fraction of the barrier is consumed. The resulting binary aluminides are also the most aluminum-rich phases obtainable, according to equilibrium phase diagrams.[32] Raising the anneal temperature to 450 °C slightly increases the diffracted x-ray intensities, but does not produce any new phases. During annealing at 500 °C, additional reflections from W $(Si,Al)_2$ arise from the $W_{80}Si_{20}$/Al and $W_{44}Si_{56}$/Al systems. In the $Mo_{74}Si_{26}$/Al system, reflections from Mo_4Al_{17} are borne from annealing at 550 °C. Consistent with total consumption of the barrier, all traces of an amorphous diffraction halos from the barriers vanish for all silicides during annealing at 550 °C, with the exception of the $Ta_{80}Si_{20}$ system.

Backscattering adds complementary information to the above x-ray-diffraction analyses. Figure 1 shows ^{4}He backscattering spectra from the ⟨Si⟩/$Mo_{74}Si_{26}$/Al, ⟨Si⟩/$W_{80}Si_{20}$/Al, and ⟨Si⟩/$W_{44}Si_{56}$/Al systems before and after annealing. Spectra of metallizations including the $Ta_{80}Si_{20}$ barrier can be found in a previous work.[27] A slight instability is detectable by backscattering in all of the systems annealed at 450 °C, which indicates that the reaction products uncovered by x-ray diffraction after annealing at 450 °C consume only a small portion of the barriers. The reaction of the bilayers proceeds somewhat further during heat treatment at 500 °C. Annealing at 550 °C completely consumes the barrier through reaction with migration of W or Mo to the surface. The backscattering yield ratio of the barrier metal to aluminum at the surface with respect to the silicon substrate is consistent with the phases $MoAl_{12}$ and WAl_{12} for the $Mo_{74}Si_{26}$ and $W_{80}Si_{20}$ systems.

The 130 nm amorphous silicide barriers with 350 nm Al overlayers were also tested on shallow-junction diodes. Although the large-area diodes do not capture all possible barrier failure modes found in today's submicron metallizations (e.g., barrier cracking at the corners of vias), they provide a practical and very sensitive assessment of planar barriers. A single weak spot over the 250×250 μm^2 area is enough to cause the metallization to fail. 42 diodes from a given barrier/Al metallization were tested after annealing at a given temperature. A metallization was deemed "stable" if the annealing did not produce any large (>5%) increase in the reverse current at −4 V in any of the 42 diodes with respect to diodes annealed at 250 °C/30 min. The as-deposited diodes typically had reverse current densities in the mid-10^{-7} A/cm^2 range; heat treatment at 250 °C served to remove defects and lower the reverse currents into the 10^{-8} A/cm^2 range. The diode results for the amorphous silicide barriers are summarized in Table I under the heading, "Max. stability temp." An explicit histogram profile is given in Fig. 2 for the ⟨Si⟩/$W_{80}Si_{20}$/Al system, which is stable up to 400 °C/30 min. The other silicide systems are also stable up to 400 °C/30 min.

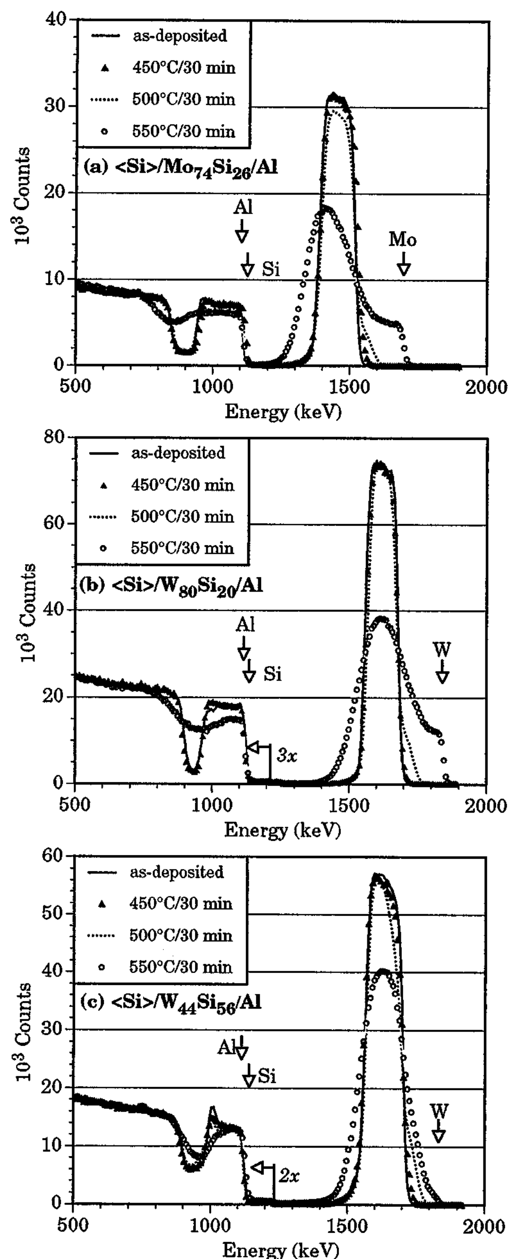

FIG. 1. 2 MeV $^4He^{++}$ backscattering spectra of the ⟨Si⟩/$Mo_{74}Si_{26}$/Al, ⟨Si⟩/$W_{80}Si_{20}$/Al, and ⟨Si⟩/$W_{44}Si_{56}$/Al systems before and after annealing in vacuum for 30 min at 450, 500, and 550 °C. The respective target tilt and scattering angles are 7° and 170°.

B. M–Si–N barriers

Because of their superior ability in blocking Al diffusion in our diode tests, barriers that are heavily laden with nitrogen are predominantly discussed. Like their silicide counterparts, most of the ternary nitride barriers listed in Table I also contain approximately 2 at. % each of argon and oxygen. The Mo–Si–N barriers, however, harbor 4–5 at. % of oxygen. Adding nitrogen to the silicides also produces a monotonic increase in resistivity. In Table I, the listed nitridedbarriers have resistivities ranging from 625 to 1800 $\mu\Omega$ cm. Annealing the barriers at 700 °C for 1 h in vacuum produces little change in the resistivity of the listed Ta–Si–N and

Downloaded¬01¬Jun¬2006¬to¬131.215.240.9.¬Redistribution¬subject¬to¬AIP¬license¬or¬copyright,¬see¬http://jap.aip.org/jap/copyright.jsp

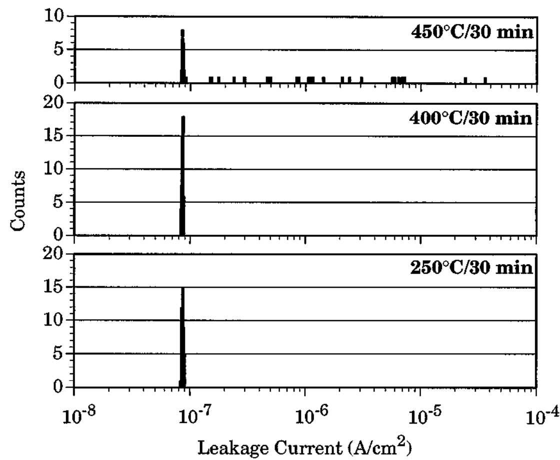

FIG. 2. Reverse current histograms of the $W_{80}Si_{20}$ (130 nm)/Al (350 nm) system on shallow n^+p junction diodes after a 30 min heat treatment at 250, 400, and 450 °C. The reverse bias is −4 V.

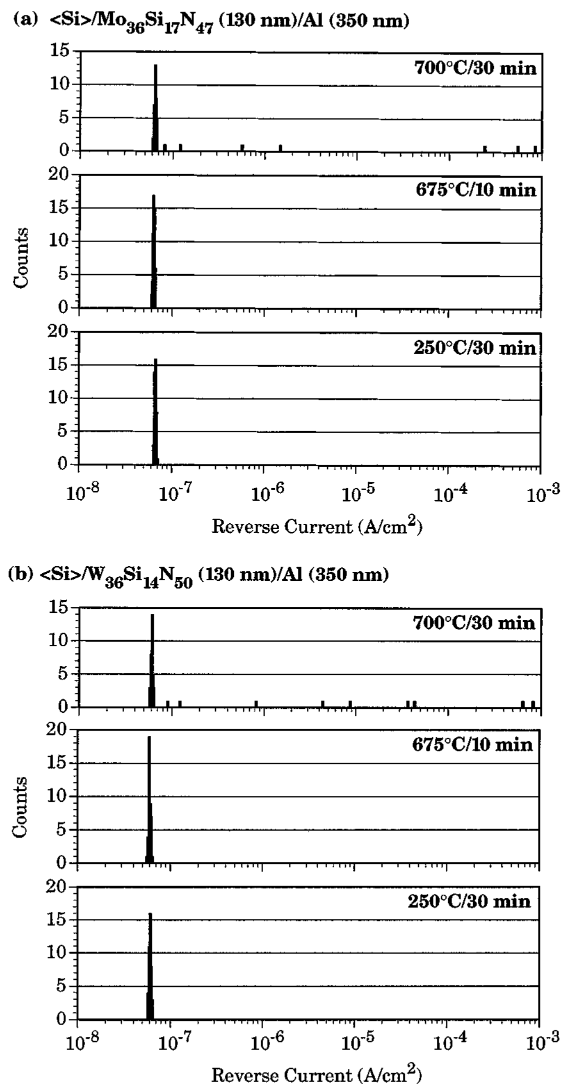

FIG. 4. Reverse current histograms of the (a) $Mo_{36}Si_{17}N_{47}$/Al, and (b) $W_{36}Si_{14}N_{50}$/Al metallizations on Si diodes biased at −4 V.

W–Si–N barriers, but does induce a 15% drop in the resistivity of $Mo_{36}Si_{17}N_{47}$ films. The crystallization temperatures of the nitrided barriers are all in excess of 750 °C.[33]

X-ray results of the M–Si–N/Al bilayers on silicon and oxidized silicon substrates are given in Table II. $W_{24}Si_{36}N_{40}$, produced from the WSi_2 target, reacts with Al already at 500 °C. Backscattering spectra verify the instability in Fig. 3. Like the reacted silicides, the ratios of the W and Al surface signals are consistent with the phase WAl_{12} in samples annealed at 550 °C. The tested compositions from the W_5Si_3 and Mo_5Si_3 targets were less reactive. As listed in Table II, $W_{41}Si_{17}N_{42}$ films did not appear to react with Al at 500 °C. Increasing the nitrogen content to approximately 50 at. % significantly improves the stability. No reaction is observed for $W_{14}Si_{36}N_{50}$ and $Mo_{17}Si_{15}N_{48}$ barriers with Al overlayers by annealing at 600 °C for 2 h. After heat treatment at 625 and 700 °C for 2 h extremely faint reflections from polycrystalline Si arise along with the strong diffraction from the amorphous barrier and Al.

According to tests on 42 diodes, 130 nm $W_{24}Si_{36}N_{40}$ films sputtered from the WSi_2 target are able to prevent a 350 nm Al overlayer from spiking the silicon substrate only up to 500 °C for 30 min. From the x-ray and backscattering results previously mentioned, the barrier appears to fail at 550 °C through reaction with aluminum. Showing remarkable improvement, the nitrogen-rich films produced from the M_5Si_3 targets prevent electrical degradation above the melting point of aluminum, 660 °C. Both the ⟨Si⟩/$Mo_{36}Si_{17}N_{47}$/Al and ⟨Si⟩/$W_{36}Si_{14}N_{50}$/Al systems are electrically stable for 10 min at 675 °C, as shown in Fig. 4 and summarized in Table I. A full 30 min heat treatment at 675 °C did cause a few of the 42 diodes to sustain large increases in reverse current. Even after annealing at 700 °C, the majority of the diodes still maintain their 10^{-8} A/cm^2 reverse currents. As previously published, $Ta_{36}Si_{14}N_{50}$ films prevent electrical degradation from Al interaction at temperatures in excess of 675 °C as well.[28]

Figure 5 shows a scanning electron micrograph of resolidified, beaded aluminum on the $W_{36}Si_{14}N_{50}$ and $Mo_{36}Si_{17}N_{47}$ barriers on Si diodes after annealing at 675 °C. 5 keV energy-dispersive analysis of x rays in the SEM does not indicate any large interaction of the Al with the barrier or

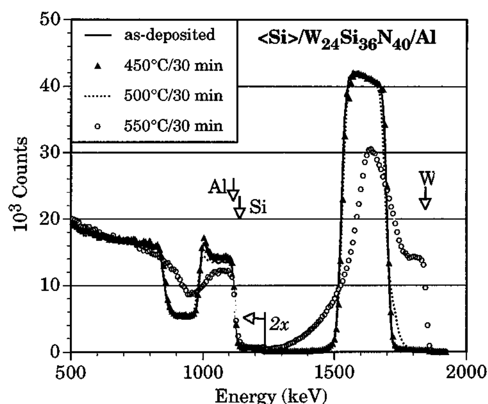

FIG. 3. 2 MeV backscattering spectra of ⟨Si⟩/$W_{24}Si_{36}N_{40}$/Al before and after 30 min annealing at 450, 500, and 550 °C.

Downloaded¬01¬Jun¬2006¬to¬131.215.240.9.¬Redistribution¬subject¬to¬AIP¬license¬or¬copyright,¬see¬http://jap.aip.org/jap/copyright.jsp

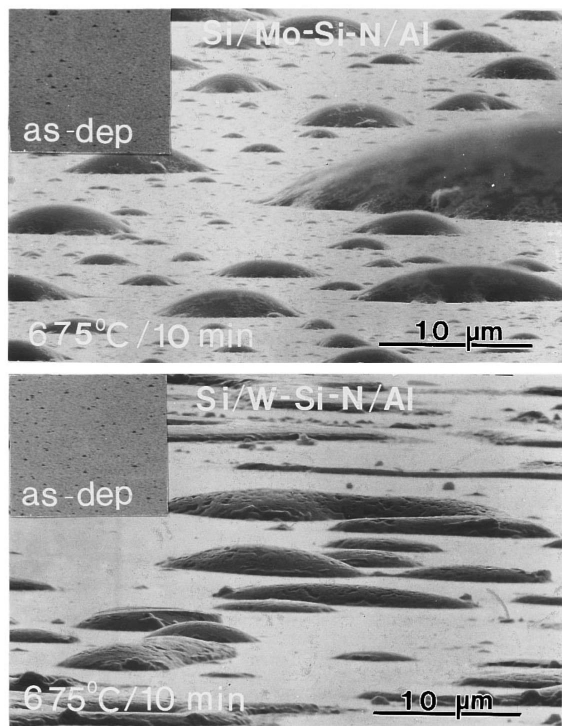

FIG. 5. Secondary electron images of the ⟨Si⟩/$Mo_{36}Si_{17}N_{47}$/Al and ⟨Si⟩/$W_{36}Si_{14}N_{50}$/Al metallizations before and after a 675 °C/10 min heat treatment. The incident beam energy is 20 keV. The sample tilt angle is approximately 80°.

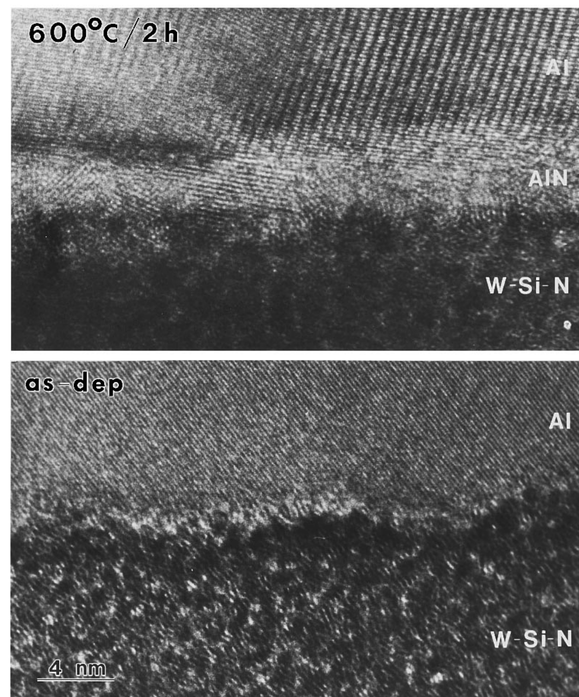

FIG. 6. High-resolution transmission electron micrographs of the as-deposited (bottom) and 600 °C/2 h annealed (top) $W_{36}Si_{14}N_{50}$/Al bilayers. The apparent interfacial roughness was caused by sample preparation.

Si substrate. Glancing-angle spectra obtained from the beads revealed only the presence of Al. Normal-direction analysis away from the beads gave strong barrier and substrate signals along with faint Al peaks. Based on the shallow geometry of the resolidified beads, Al plausibly wets the barrier.

High-resolution transmission electron micrographs of $W_{36}Si_{14}N_{50}$/Al bilayer cross sections are given in Fig. 6. In the as-deposited sample, lattice fringes from the Al extend completely to the barrier. However, in the sample annealed for 2 h at 600 °C, the aluminum fringes terminate about 3 nm from the barrier. Close inspection of the interface reveals faint fringes from a nanophase layer. Microdiffraction of the layer bears weak spots consistent with the (100), (002), and (102) reflections of wurtzite-structured AlN. It is entirely possible that the reflections are, in fact, from an aluminum oxynitride, given the ability of AlN to dissolve about 7 at. % oxygen, according to work on the AlN–Al_2O_3 system.[34,35] Based on the work of Schuster and Nowotny,[36,37] AlN does not dissolve the group V–VI transition metals, thus the reaction layer may contain little transition metal. The high degree of electron transmission through the interfacial layer shown in Fig. 6 supports this premise. The AlN is essentially invisible here by x-ray diffraction because of the small amount, disordered nature, and weak scattering power of the compound. In one of the electron microdiffraction patterns, faint points matching the (220) reflection of Si were observed. As previously mentioned, the polycrystalline Si is also detected by x-ray diffraction after annealing at 625 °C.

As an attempt to measure the diffusivity of Al in the ternary barriers, SIMS was performed on ⟨Si⟩/SiO_2/$Ta_{36}Si_{14}N_{50}$ (100 nm)/Al (7 nm)/$Ta_{36}Si_{14}N_{50}$ (50 nm) sandwich structures before and after annealing at 500–700 °C. Even after heat treatment at 700 °C for 10 h, there is virtually no change in the Al profile with respect to profile obtained from as-deposited samples. Consistent with the TEM results, the thin Al layer may react to form a self-sealing interface with the barrier, thus containing the Al. Impurities at the interface and/or in the Al may be another possible explanation for the apparent lack of diffusion of Al through the barrier, an interpretation that we cannot exclude. No attempt was made to measure an oxygen profile.

IV. DISCUSSION

Amorphous transition-metal silicide films are unimpressive barriers for blocking interaction of aluminum with silicon. As shown by x-ray diffraction, the barriers react with Al to form $MoAl_{12}$, WAl_{12}, and $TaAl_3$ during annealing at only 350 or 400 °C. According to the diode evaluations, the barriers are breached during heat treatment at 450 °C. ^{4}He backscattering proved to be the least sensitive test of the stability of the amorphous silicide/Al metallizations. In most instances, annealing at 450 °C provided only a small change in spectra compared with spectra obtained from as-deposited samples. Consequently, the reaction products found by x-ray diffraction are probably local protrusions into the barrier. Similar behavior has been observed in some studies of (Mo, Ta, and W)-silicide/Al systems.[25,38–43]

The addition of nitrogen to the transition-metal silicide systems significantly improves the barrier performance. All of the ternary systems with approximately 50 at. % nitrogen are able to prevent Al from spiking into the shallow-junction

Downloaded¬01¬Jun¬2006¬to¬131.215.240.9.¬Redistribution¬subject¬to¬AIP¬license¬or¬copyright,¬see¬http://jap.aip.org/jap/copyright.jsp

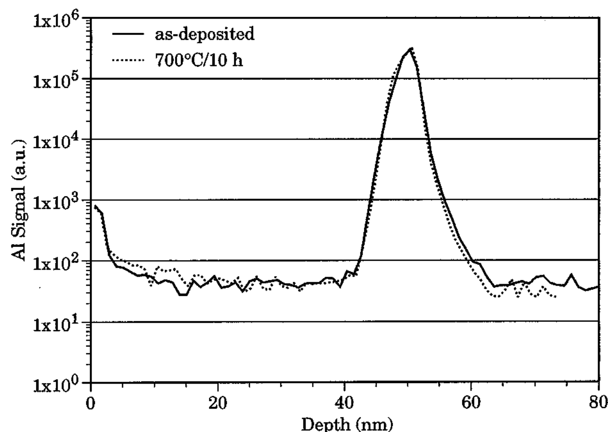

FIG. 7. Aluminum signal from SIMS of the $SiO_2/Ta_{36}Si_{14}N_{50}$ (100 nm)/Al(7 nm)/$Ta_{36}Si_{14}N_{50}$ (50 nm) structures. The spectrometer was a Cameca model 4F; the beam was 5.5 keV Ar^+.

diodes at temperatures in excess of the melting point of Al, 660 °C. Based on the transmission electron microscopy observations of the W–Si–N/Al system, the stability is attributable, in part, to a self-sealing AlN layer which grows at the barrier/Al interface. A literature search provides no information on the diffusivity of Al in AlN, but the values are evidently very low based on the low diffusivity shown in Fig. 7. Because a large percentage of the diodes survives a 700 °C annealing, the failure is most likely local in nature: Al probably channels through local weak spots and/or particles in the barrier films.

Analogously, Al dissociates both Si_3N_4 and $W_{36}Si_{14}N_{50}$ to form poly-Si and a thin interfacial layer of AlN.[29–31] The thin AlN acts as a diffusion barrier to retard further reaction. Structurally, the nitrogen-rich M–Si–N films appear to be a combination of M nitrides and silicon nitride, albeit with no long-range order, based on extended-energy-loss-fine-structure (EXELFS) measurements.[44,45] Aluminum thus appears to dissociate the SiN_x constituent preferentially rather than the transition-metal nitride component. The close proximity the of local SiN_x regions in the amorphous structure ensures that the AlN layer is continuous. Otherwise, transition-metal aluminides would likely be observed. Paradoxically, the Mo, W, and Ta binary nitrides are known to be quite reactive with Al,[4–8,36,37] assuming the interface to be free of native oxides.[46] Conditionally, for the preferential attack of SiN_x to occur, the M–Si–N systems apparently need to be nearly saturated with nitrogen. Figure 8 shows the tested compositions plotted on the ternary phase diagrams for systems primarily at 1000 °C.[29] (Although binary molybdenum and tungsten nitrides do not exist at 1000 °C without a nitrogen ambient, they are included here for completeness and their relevance at lower temperatures. Strictly speaking, the Mo–Si_3N_4 tie line also does not exist at 1000 °C, but the reaction is sluggish.[29,47] Moreover, Gibbs free-energy data indicate that Mo and Si_3N_4 are thermodynamically compatible at lower temperatures mainly because of the large negative entropy of Si_3N_4.[48]). For the tested compositions near or on the nitrogen-poor side of the M_2N–Si_3N_4 tie line, namely $W_{41}Si_{17}N_{42}$ and $W_{24}Si_{36}N_{40}$, the films react to form the M

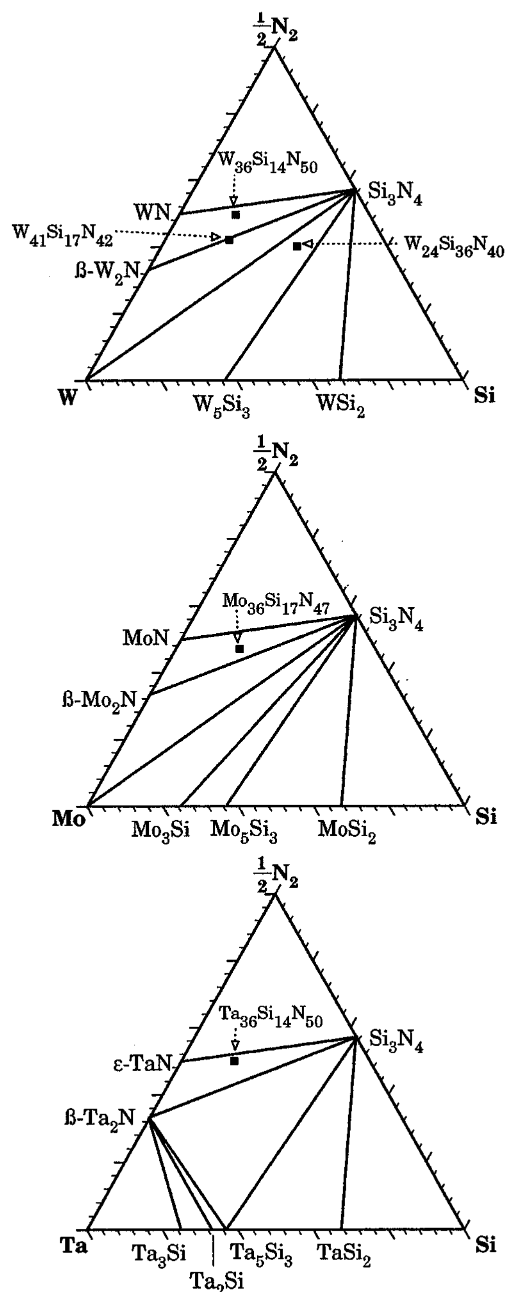

FIG. 8. Ternary phase diagrams of the W–Si–N, Mo–Si–N, and Ta–Si–N systems. The homogeneity ranges of the phases are not included.

aluminides (WAl_{12}). Increasing the nitrogen content to nearly 50 at. % (i.e., near the MN–Si_3N_4 tie line), as the case with $Mo_{36}Si_{17}N_{47}$, $Ta_{36}Si_{14}N_{50}$, and $W_{36}Si_{14}N_{50}$ films, prevents the formation of the M aluminides and instead produces the self-sealing AlN layer. Conceivably, the nearly saturated transition-metal nitride components lend some nitrogen to the formation of the AlN layer.

V. CONCLUSION

When nearly saturated with nitrogen, the Mo–Si–N, Ta–Si–N, and W–Si–N thin films are effective diffusion barriers for molten aluminum. The exceptional degree of stability can be credited, in part, to a very thin, self-limiting AlN layer

Downloaded¬01¬Jun¬2006¬to¬131.215.240.9.¬Redistribution¬subject¬to¬AIP¬license¬or¬copyright,¬see¬http://jap.aip.org/jap/copyright.jsp

that grows on the barrier/Al interface. Similar behavior is observed in the Si_3N_4/Al system. Because of high stability, very thin M–Si–N barriers (e.g., 10 nm) should suffice for device applications with no degradation in stability. Ancillary studies are currently underway to study the effect of the AlN layer on the electrical contact resistance of M–Si–N/Al metallizations. Although not addressed in this article, these barriers may show further versatility in very large scale integrated planarization processing and composite material fabrication.

ACKNOWLEDGMENTS

The authors thank Bruce Gorris for technical assistance. Financial support for this work was provided by the Army Research Office. The shallow-junction diodes used in our evaluations were fabricated by Sandia National Laboratories, Albuquerque. J.S.R. gratefully acknowledges a fellowship from the Intel Foundation.

[1] R. J. Schutz, Thin Solid Films **104**, 89 (1983).
[2] N. Cheung, H. von Seefeld, and M.-A. Nicolet, in *Proceedings of the Symposium on Thin Film Interfaces and Reactions*, edited by J. E. E. Baglin and J. Poate (The Electrochemical Society, Princeton, NJ, 1980), Vol. 80-2, p. 323.
[3] C. Y. Ting and M. Wittmer, Thin Solid Films **96**, 327 (1982).
[4] H. P. Kattelus, E. Kolawa, K. Affolter, and M.-A. Nicolet, J. Vac. Sci. Technol. A **3**, 2246 (1985).
[5] F. C. T. So, E. Kolawa, Z.-A. Zhao, and M.-A. Nicolet, Thin Solid Films **153**, 507 (1987).
[6] S. E. Hörnström, A. Charai, O. Thomas, L. Krusinelbaum, P. M. Fryer, J. M. E. Harper, S. Gong, and A. Robertsson, Surf. Interface Anal. **14**, 7 (1989); A. Charai, S. E. Hörnström, O. Thomas, P. M. Fryer, and J. M. E. Harper, J. Vac. Sci. Technol A **7**, 784 (1989).
[7] V. P. Anitha, A. Bhattacharya, N. G. Patil, and S. Major, Thin Solid Films **236**, 306 (1993).
[8] M. A. Faroq, S. P. Murarka, C. C. Chang, and F. A. Baiocchi, J. Appl. Phys. **65**, 3017 (1989).
[9] L. Krustin-Elbaum, M. Wittmer, C.-Y. Ting, and J. J. Cuomo, Thin Solid Films **104**, 81 (1983).
[10] J. R. Shappirio and J. J. Finnegan, Thin Solid Films **107**, 81 (1983).
[11] J. R. Shappirio, J. J. Finnegan, R. A. Lux, and D. C. Fox, Thin Solid Films **119**, 23 (1984).
[12] E. Kolawa, J. M. Molarius, W. Flick, C. W. Nieh, L. Tran, M.-A. Nicolet, F. C. T. So, and J. C. S. Wei, Thin Solid Films **166**, 29 (1988).
[13] E. Kolawa, X. Sun, J. S. Reid, J. S. Chen, M.-A. Nicolet, and R. P. Ruiz, Thin Solid Films **236**, 301 (1993).
[14] F. C. T. So, E. Kolawa, S. C. W. Nieh, Z.-A. Zhao, and M.-A. Nicolet, Appl. Phys. A **45**, 265 (1988).
[15] E. Kolawa, C. Garland, L. Tran, C. W. Nieh, J. M. Molarius, W. Flick, M.-A. Nicolet, and J. Wei, Appl. Phys. Lett. **53**, 2644 (1988).
[16] H.-Y. Yang, X.-A. Zhao, and M.-A. Nicolet, Thin Solid Films **158**, 45 (1988).
[17] M. Wittmer, J. Appl. Phys. **53**, 1007 (1982).
[18] M. Eizenberg, S. P. Murarka, and P. Heimann, J. Appl. Phys. **54**, 3195 (1983).
[19] M. Eizenberg, R. Brener, and S. P. Murarka, J. Appl. Phys. **55**, 3799 (1984).
[20] A. Appelbaum and S. P. Murarka, J. Vac. Sci. Technol. A **4**, 637 (1986).
[21] I. Suni, M.-A. Nicolet, C. S. Pai, and S. S. Lau, Thin Solid Films **107**, 73 (1983).
[22] F. C. T. So, X.-A. Zhao, E. Kolawa, J. L. Tandon, M. F. Zhu, and M.-A. Nicolet, Mater. Res. Soc. Symp. Proc. **54** (1986).
[23] L.-S. Hung, E. G. Colgan, and J. W. Mayer, J. Appl. Phys. **60**, 4177 (1986).
[24] F. W. Saris, L.-S. Hung, M. Nastasi, J. W. Mayer, and B. Whitehead, Appl. Phys. Lett. **46**, 646 (1985).
[25] O. Thomas, F. M. d'Heurle, and S. Delage, J. Mater. Res. **5**, 1453 (1990).
[26] J. D. Wiley, J. H. Perepezko, J. E. Nordman, and K.-J. Guo, IEEE Trans. Ind. Electron. **IE-29**, 154 (1982).
[27] E. Kolawa, J. M. Molarius, C. W. Nieh, and M.-A. Nicolet, J. Vac. Sci. Technol. A **8**, 3006 (1990).
[28] E. Kolawa, P. J. Pokela, J. S. Reid, J. S. Chen, and M.-A. Nicolet, Appl. Surf. Sci. **53**, 373 (1991).
[29] *Phase Diagrams of Ternary Boron Nitride and Silicon Systems*, edited by P. Rogl and J. C. Schuster (ASM International, Materials Park, OH, 1992).
[30] R. Brener, F. Edelman, and E. Y. Gutmanas, Appl. Phys. Lett. **54**, 901 (1989).
[31] M. Naka, H. Mori, M. Kubo, I. Okamoto, and H. Fujita, J. Mater. Sci. Lett. **5**, 696 (1986).
[32] T. B. Massalski, *Binary Alloy Phase Diagrams*. 2nd ed. (ASM International, Materials Park, OH, 1990).
[33] J. S. Reid, E. Kolawa, R. P. Ruiz, and M.-A. Nicolet, Thin Solid Films **236**, 319 (1993).
[34] G. A. Slack, Acta Crystallogr. B **21**, 2281 (1979).
[35] M. Hilber and S. Johnsson, Z. Metallkd. **88**, 720 (1992).
[36] J. C. Schuster and H. Nowotny, Z. Metallkd. **76**, 728 (1985).
[37] J. C. Schuster and H. Nowotny, J. Mater. Sci. **20**, 2787 (1985).
[38] S. Fukada, M. Suwa, Y. Koubuchi, and J. Onuki, J. Vac. Sci. Technol. B **9**, 215 (1991).
[39] F.-M. Yang and M.-C. Chen, J. Vac. Sci. Technol. B **11**, 744 (1993).
[40] Y. K. Fang and H. M. Yang, IEEE Trans. Electron Devices **ED-35**, 706 (1988).
[41] T. Hara, H. Hayashida, S. Takahashi, and A. Yamanoue, Thin Solid Films **177**, 9 (1989).
[42] T. Kikkawa and N. Endo, J. Appl. Phys. **70**, 2370 (1991).
[43] G. J. van Gurp, J. L. C. Daams, A. van Oostrom, L. J. M. Augustus, and Y. Tamminga, J. Appl. Phys. **50**, 6915 (1979).
[44] J. S. Reid, Ph.D. thesis, California Institute of Technology, 1995.
[45] J. S. Reid and C. C. Ahn (unpublished).
[46] J. M. E. Harper, S. E. Hörnström, O. Thomas, A. Chairai, and L. Krusin-Elbaum, J. Vac. Sci. Technol. A **7**, 875 (1989).
[47] J. C. Schuster, J. Mater. Sci. **23**, 2792 (1988).
[48] I. Barin, *Thermochemical Data of Pure Substances* (VCH, Weinheim, Germany, 1989).

Downloaded¬01¬Jun¬2006¬to¬131.215.240.9.¬Redistribution¬subject¬to¬AIP¬license¬or¬copyright,¬see¬http://jap.aip.org/jap/copyright.jsp